Materials Research Proceedings 29 (2023) 456-471 https://doi.org/10.21741/9781644902516-52

Detection and characterization of chloride induced stress corrosion cracking on SS304 under perlite thermal insulation

SURESH Nuthalapati[1, a] K.E. Kee[1,b*], SRINIVASARAO Pedapati[1,c]

Department of Mechanical Engineering, Universiti Teknologi PETRONAS, Malaysia

suresh_20001751@utp.edu.my[a], keekokeng@utp.edu.my[b], srinivasa.pedapati@utp.edu.my[c]

Keywords: SS304, Sensitization, Grain Size, Perlite Thermal Insulation, Pitting Corrosion, Crack Evaluation

Abstract. Austenitic stainless steel (ASS) type SS304 has been extensively employed in various sectors because of its good structural strength and corrosion resistance. These steels are susceptible to chloride-induced stress corrosion cracking (CISCC), particularly by the effect of chloride corrosive environment under thermal insulation. Corrosive environment formed by external sources or condensation due temperature differences under thermal insulation as a result of inadequate maintenance or unfavourable climatic conditions. It causes localised corrosion and leads to catastrophic failure under the action of tensile stress. The objective of the research was to detect the chloride-induced stress corrosion cracking on SS304 under thermal insulation. This study simulated a real corrosive environment using water containing chloride ions on U-bend samples to estimate the susceptibility and assess CISCC under the drip test method. SS304 as-received (AR) and sensitized (SEN) over-stressed U-bend samples were tested as per ASTM C692 standard. Samples were exposed to 0.1, 1.0, and 3.5 wt. % of NaCl concentrations under perlite thermal insulation and tested at 90°C. Under high chloride concentrations, SEN samples were susceptible more and showed little evidence of crack initiation. The rest of the concentrations showed no evidence of crack, but they showed tiny localized corrosion near the dripping zone. The characteristics of the material structure and the corrosion mechanism were described in a pictorial view.

Introduction

Austenitic stainless steels (ASSs) are widely utilized in various industries such as oil, gas, petrochemical, food, nuclear etc. because of their remarkable corrosion resistance and favourable mechanical properties [1], [2]. However, ASSs are more susceptible to CISCC in a chloride-containing environment. This environment can damage the passive film, resulting in pitting and leads to cracking under mechanical loading [3]. Generally, the stress corrosion cracking (SCC) failures induced by presenting chlorides from external sources such as rain, coastal fog, leaks etc., and thermal insulation are likely to develop. These are the major sources to form chlorides on the metal surface to initiate cracks [4]. Sodium chloride (NaCl) is the most frequent offender due to its high solubility and extensive distribution. This is most common but not much aggressive. Under thermal insulation, the concentration of chloride deposits on the metal surface is still controversial. But it is mostly affected by the temperature transformations on the metal surface. Although it was difficult to estimate the necessary chloride concentration for SCC, but it was observed remarkably low levels of chloride (10ppm) in the solution [5].

Thermal insulation is essential for economical and safety concerns in various industries. The continuous use of insulated components like pipes or pressure vessels requires an assessment to define their damages. Predominantly those industries located close to unfavourable environments, ASSs might be more susceptible to corrosion such as pitting, stress corrosion cracking, crevice corrosion and intergranular attack [6]. Furthermore, CISCC occurs due to the generation of moisture under thermal insulation which means the interface between insulation and the surface

of pipe or equipment. There is a temperature differential that leads to condensation when the material surface temperature below the atmospheric dew point. The condensed chloride ions with other dissolved particles were unfree in the annular space. Then, over time the metal surface will corrode, particularly for surfaces without coating [7].

Under the insulation, CISCC is possible in the presence of tensile stress when the chlorides or other contaminants are present in the range of 50ºC-150ºC temperature [8]. No cracking will take place if the tensile stress is removed or significantly decreased. The majority of CISCC cracks are quite small and exhibit considerable crack branching in a transgranular path that is mostly uninterrupted by grain boundaries. The possible cracks propagate along the grain boundary indicating that the steel is in a sensitised state when loses its integrity [9]. The ASSs becomes sensitive as a result of sensitization or heat-affected area from the perspective of the welding or heat treatment applications. When these applications allow holding or decreasing the temperature range between 900ºC and 480ºC, leads to chromium depletion at the grain boundary due to the formation of chromium carbides [10], [11]. It could be affected to increase the microhardness slightly as well grain growth [12].

Perlite thermal insulation has been used in various insulation applications because of its unique properties, and it is non-flexible granular type material [13]. In a recent experimental work under perlite thermal insulation, SS304L did not show any evidence of CISCC [14]. Despite numerous studies done on the field of SCC under thermal insulation, there are still many issues and difficulties. SCC under thermal insulation remained one of the biggest challenges in various industries [15]. Many researchers focused on SCC detection and its mechanism without thermal insulation, only few worked on insulated components. As result, there is no clear understanding of the CISCC vulnerability, mechanism and characteristics. SCC mechanism has been assessed in different testing methods with various corrosive solutions [16]. The studies reported that static tensile stress combined with active corrosion causes fractures, which eventually lead to catastrophic damage to the sensitive component [17], [18]. These unexpected failures cause dangerous explosions leads to economic loss for the oil, gas and other chemical industries. According to a 2016 NACE international study, the global cost of corrosion was expected to be 2.5 trillion dollars, or 3.4 percent of the world's GDP in 2013 [19]. Consequently, periodical inspection is required to detect the damages or fractures under the insulation so as can forecast the potential hazards.

In the present study, the effect of the combined action of chloride concentration and tensile stress on the SCC susceptibility has been studied systematically for SS304 AR and SEN U-bend samples using drip test apparatus simulating the corrosive environment. Microstructures of different test samples were also studied to reveal its damage mechanism.

Material and Methods

Sample Preparation:

AR and SEN (SS304) samples were used for drip test with a hot fluid circulating pipe-spool. Based on the pipe-spool external diameter, samples were designed and cut as dimensions of 3^{t}x 25^{w}x 220^{l} in millimeters from the long bar. AR flat samples were heat treated by soaking in muffle furnace for 3 hours at constant temperature of 649ºC and cooled in furnace itself as per ASTM C 692 standard [20]. Both samples were prepared for their microstructure followed by grinding-polishing and electrolytic etching according to ASTM E3 [21] and ASTM A262 [22] respectively. The composition elements of SS304 AR and SEN samples were presented in Table 1 as identified by Hitachi table top SEM (TM3000) with energy dispersive X-ray (EDX) spectroscopy (Bruker Quantax 70) system according to ASTM E572 [23]. For the tensile test used a sub-sized flat specimen with 3mm thickness as per ASTM E08M [24]. Also, Vickers microhardness mechanical test was performed on 3 mm thickness of 30x30 mm square plate using Leco microhardness tester (LM 247AT) according to the ASTM E384 standard [25]. The hardness tester was equipped with

diamond pyramidal indenter with 1Kgf load at maximum. The mechanical properties of AR and SEN samples are presented in Table 2 in accordance with ASTM A240 [26].

Table 1: Chemical compositions of SS304 As received and sensitized

Elements	As received	ASTM A240	Sensitized	ASTM A240
C	0.091 ± 0.002	>0.08	0.12 ± 0.003	>0.08
Mn	1.83 ± 0.1	<2.00	1.94 ± 0.1	<2.00
P	0.058 ± 0.03	>0.045	0.037 ± 0.05	<0.045
S	0.036 ± 0.02	>0.030	0.042 ± 0.02	>0.030
Si	0.48 ± 0.05	<0.75	1.09 ± 0.04	>0.75
Cr	18.23 ± 0.2	18.00-20.00	18.92 ± 0.1	18.00-20.00
Ni	8.45 ± 0.04	8.00-10.50	8.90 ± 0.06	8.00-10.50
N	0.16 ± 0.02	>0.10	0.08 ± 0.01	<0.10

Table 2: Mechanical properties of SS304 AR and SEN samples

Mechanical Properties	As-received	ASTM A240	Sensitized	ASTM A240
Yield strength (MPa)	363.38	>205	346.26	>205
Tensile strength (MPa)	687.51	>515	681.05	>515
Micro-Hardness	206.3HB (217.2HV)	>201HB (HV≈1.05HB)	215.1HB (226.5HV)	>201HB (HV≈1.05HB)

The test samples were prepared according to the ASTM G30 [27]. Geometrical dimensions were depicted in a graphical representation of mechanical loading assembly using two-stage method to make U-bend as shown in Figure 1 (a). A stressed U-bend accomplished by allowing the elastic strain to relax at the first stage and followed by the second stage through tightening nut and bolt until legs held in parallel with each other. And a decent approximation of the strain (ε) was derived on an investigated area of U-bend using ε = t/2R, where, t is thickness and R is radius of the sample. Then, an appropriate value of the maximum stress was determined from the stress-strain curve of the test material. Furthermore, calculated the leg deflection as shown in Figure 1 (b) to produce the desired elastic stress using equation 1 [28].

$$\text{Deflection } (\delta) = \left[\frac{12S(2R+t)}{(L+R)\,(8R+t)(t)(E)}\right] \cdot \left[\frac{L^3}{3} + R\left(\frac{\pi L^2}{2} + \frac{\pi R^2}{4} + 2LR\right)\right] \ldots\ldots\ldots (1)$$

Where δ is the leg deflection (in), S is the applied stress (psi), E is the modulus of elasticity (psi), R is the radius of bend (in), t is the thickness of sample (in) and L is the length of the straight section (in).

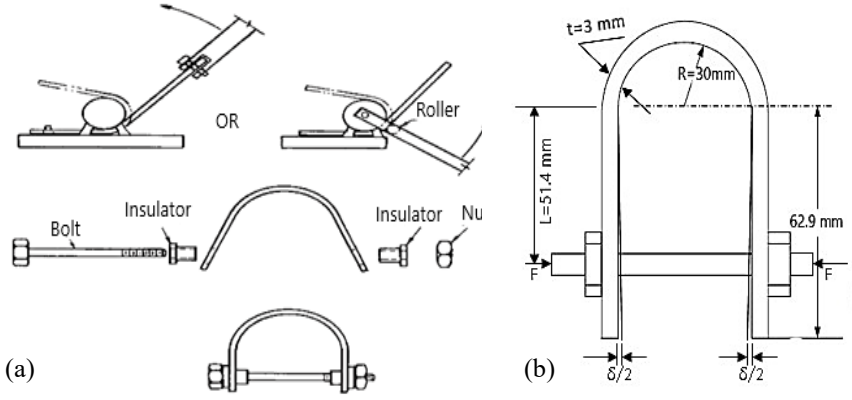

Figure 1: (a) Schematic view of a two-stage method for U-bend making [27], (b) Schematic view of leg deflection

Equipment setup:

The drip test apparatus consists of pipe-spool, oil bath circulating tank with temperature control setup, solution tank, peristaltic pump, drippers and temperature sensors for temperature readings. AR and SEN samples were placed over the two inch diameter pipe-spool as shown in Figure 2 according to the ASTM C692 [20]. The samples with pipe-spool heated by circulating silicone oil which was heated at 90ºC in an oil bath circulating tank. The pipe-spool inlet and outlet temperatures were observed through the given indicators. The perlite thermal insulation blocks as per ASTM C610 [29], selected and prepared according to the ASTM C585 standards [30]. It has a good physical properties such as density (50-150 Kg/m^3), thermal conductivity (0.057W/mK at 80 Kg/m^3), service temperature (-250-1000ºC) and thickness (25-300 mm) at 20ºC [31]. The prepared blocks were enclosed over the samples along the pipe-spool.

Sodium chloride (NaCl) solution was prepared in weight percentage as 0.1, 1.0, 3.5 with deionized water according to ASTM D1193 standard [32]. The prepared solution dripped over the insulated material by peristaltic pump which was calibrated for 21 ml per two hours. Three AR and three SEN insulated samples were tested in one attempt under three different NaCl concentrations. The test matrix as shown in Table 3, was prepared in accordance with the aforesaid test requirements in order to execute the test.

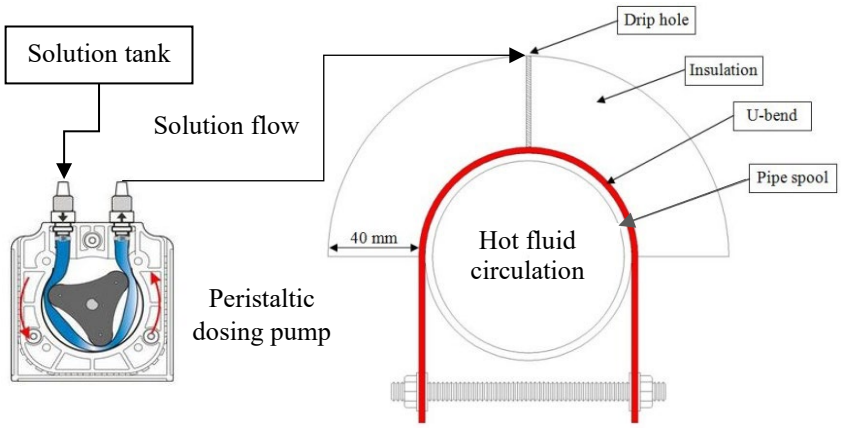

Figure 2: Line diagram of auto drip control system set up for SCC test

Materials Research Proceedings 29 (2023) 456-471 https://doi.org/10.21741/9781644902516-52

Table 3: Test process and its parameters

Test Duration	68 days					
Temperature	90 °C					
Insulation Type	Perlite					
Sample type	SS304 As-received			SS304 Sensitised		
NaCl concentration (wt.%)	3.5	1.0	0.1	3.5	1.0	0.1
Test No	AR1	AR2	AR3	SEN1	SEN2	SEN3
Evaluation	Visual, DPT, Stereo microscope, Optical microscope					

Finally, Aluminium sheet was used to cladding along the insulated pipe-spool and tied with binding wires evenly then run the test at 90ºC. During the test maintained neutral pH by adding hydrochloric acid (HCl) reagent according to the ASTM G44 [33]. Each sample has been observed periodically by using die penetrant test (DPT) and stereo microscope. Following the observation, each sample was stressed by leg deflection and then sustained the test. After completion of the test, results were analysed by using an optical microscope with suitable magnifications followed by grinding-polishing and etching. Also, used TESCAN CLARA's FESEM (Field Emission Scanning Electron Microscopy) to characterize the material structure. In addition, Vickers hardness was used to analyse the micro hardness at the centre of an investigated area by applying 1kgf load to the given indenter. The results were compared to those from the preceding tests.

Result and Discussion

Formation of Localised Corrosion:

Table 4 summarizes the periodical inspection results for as-received (AR) and sensitized (SEN) insulated SS304 samples as per test conditions. Upon removal of perlite thermal insulation block for inspection, the sample surfaces were slightly moist around the dripping zone with stains and specks of salt deposits that built-up with time as shown in Figure 3 (a). All the U-bend samples tested at 90ºC under perlite thermal insulation revealed brown rusting stains around the dripping zones except AR3 sample. For U-bend samples exposed to higher salinity i.e. 3.5 wt.% NaCl, colonies of pits were found distributed in the vicinity around the dripping zones as shown in Figure 3 (b). At the inspection time after 972 hours, only stains but no pits were observed for samples exposed to 0.1 and 1 wt% NaCl. Pitting was only found on samples under 3.5 wt% NaCl. It is well established that the presence of chloride can rupture the passive oxide film and lead to initiation of new pits [34]. At the end of 1632 hours, all samples showed varying levels of localized corrosion without cracks, except for SEN1 sample under 3.5 wt% NaCl. The severity of localized corrosion can be related to the concentration levels of NaCl and the type of samples, whereby higher NaCl concentration resulted in more severe localized corrosion. Also, the heat-sensitized samples showed more susceptibility than as-received sample to localized corrosion and stress corrosion cracking [28], [35].

Table 4: Summarized results under the test conditions

Temperature (°C)	90					
Insulation type	Perlite					
Sample Type	SS304 As-received (AR)			SS304 Sensitized (SEN)		
NaCl Concentration (%)	3.5	1.0	0.1	3.5	1.0	0.1
Test No	AR1	AR2	AR3	SEN1	SEN2	SEN3
After 72 h.	X	X	X	X	X	X
After 272±5 h.	Stains	X	X	Stains	Stains	X
After 472±5 h.	pits	Stains	X	pits	Stains with brown rust	Stains
After 672±5 h.	pits	Stains	X	pits	Stains with brown rust	Stains
After 972±5 h.	pits	Stains	X	pits	Stains with brown rust	Stains
After 1632± 5h.	pits	Stains with brown rust	Stains	SCC	Stains with brown rust	Stains with brown rust

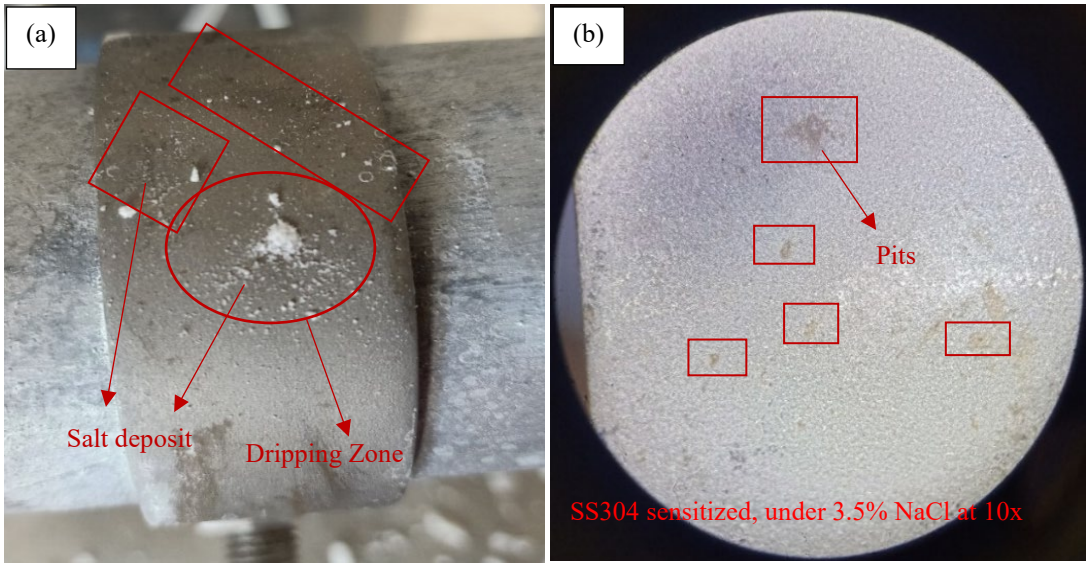

Figure 3: (a) Salt deposit observed onSEN1 sample, (b) Stereo microscope image of corroded sample

Figure 4 illustrates the progressive evolution, state of pitting for AR1 and SEN1 samples. These visuals focused on a specific pit from both samples and observed periodically. The pit area was observed to grow based on the direction of passive film dissolution around the long-standing pit. It is believed that the pit growth will eventually lead to crack formation as time progresses, as evidenced by SEN1 sample after 1632 hours as shown in Figure 4 (d). However, the AR1 sample did not produce any crack under the same test condition. This indicates the heat-sensitized SS304 is more susceptible to cracking under high chloride concentration.

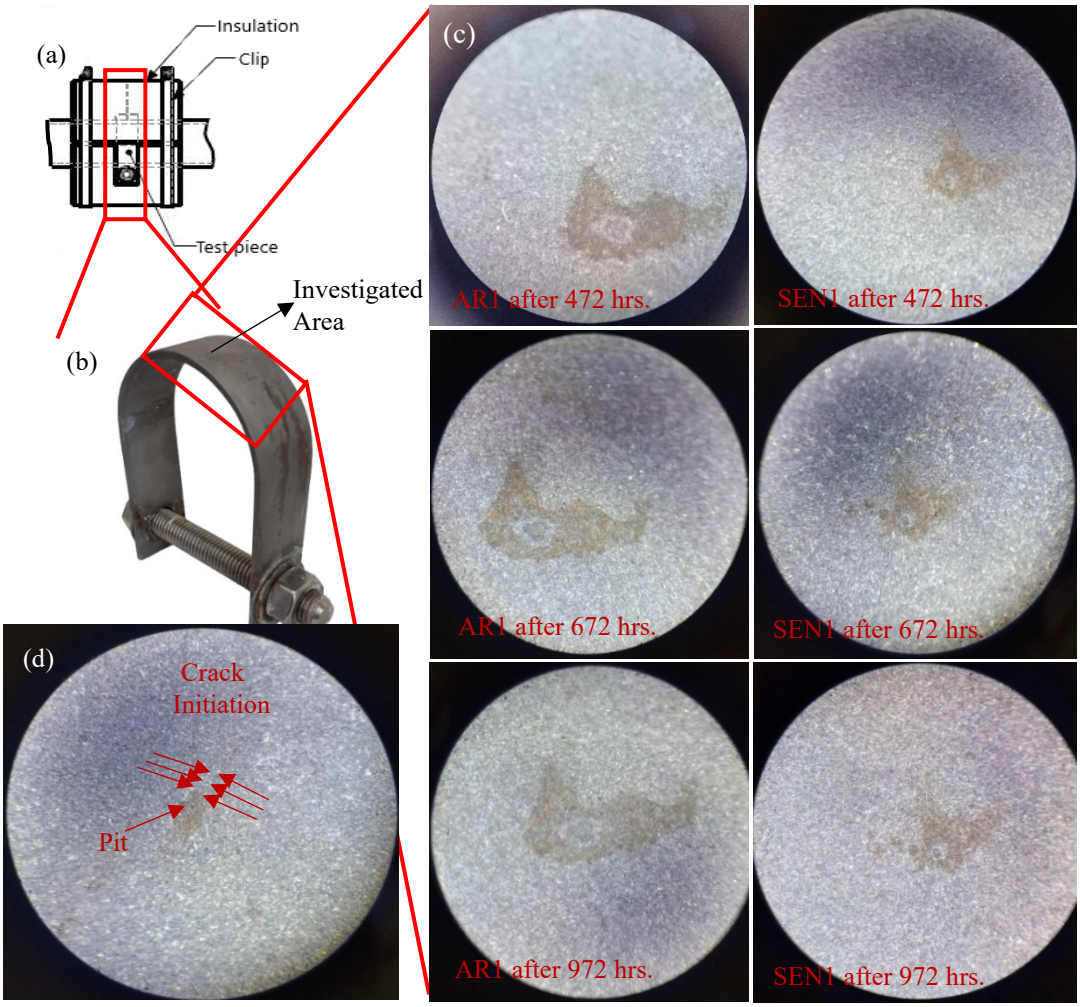

Figure 4: (a) Schematic view of U-bend covered by thermal insulation, (b) SS304 testing U-bend sample and (c) stereo microscopic images of SS304 as received (AR1) and sensitized (SEN1) samples pit variation under 3.5 wt% NaCl solution, (d) Crack initiation.

Vickers hardness observation:

Figure 5 compares the Vickers micro-hardness (HV) test results for both AR and SEN taken before test and after test. The measurement points were taken at center of U-bend apex area, and the HV reading were taken at 1mm intervals by applying 1 kg force in 10 seconds dwell period.

Before the test, the SEN sample had slightly higher average HV than AR, most likely due to carbide formation. These may impede dislocation movement after heat sensitization treatment at 649ºC. Generally, the hardness depends on the types of heat treatment process and crystal lattice dislocation at grain boundaries in relation to flow stress in the Hall-Petch relation [36]–[39]. The average HV measured after test were found to be higher than before test by 21% and 30% for AR1 and SEN1, respectively. The rise of hardness may be attributed to the 'semi-quenching' state of the samples. In the present work, the samples were heated at constant temperature (90ºC) and then quenched periodically by aqueous solution dripping to create periodic dry/wet cycle in the insulated sample. This condition would favours the formation of hard carbide compounds on the surface, thereby contributing to micro-hardness enhancement.

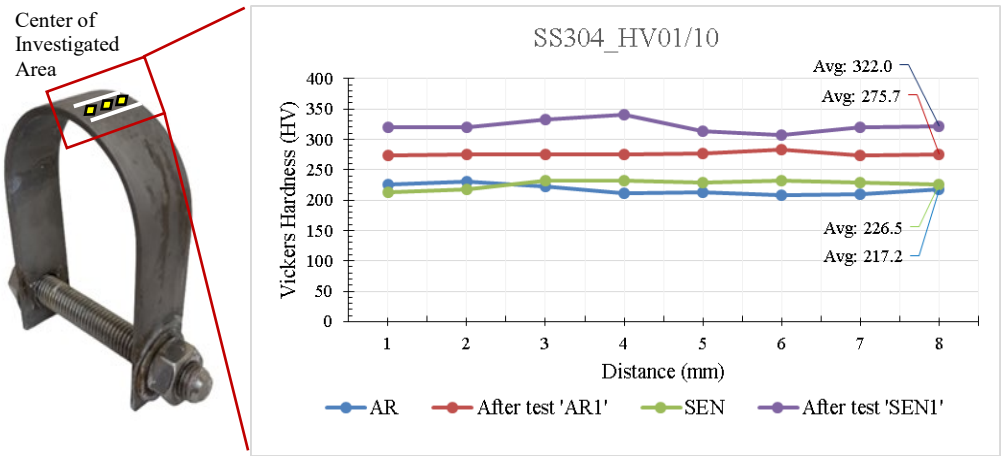

Figure 5: Micro-hardness (HV) comparison of before and after the test

Metallographic observation:

Metallography is a study of materials microstructure and can influence its physical properties, and employed in failure analysis to investigate the mechanism of corrosion and oxidation [40].

Optical microscopic observation:

Figure 6 (a), (b) represents the austenite phase with a homogeneous matrix of both samples before the test. Expected that the SEN sample shown chromium carbides (Cr_{23} C_6) in the grain boundaries, but does not completely encircle the grains. After the test, there is no much difference in structure of AR1 as shown in Figure 6 (c) but seems to be a grain size has been increased slightly. Figure 6 (d) shown, the SEN1 sample's grain boundary thickness has been increased, also observed small particles on grains supposed to be σ (Fe-Cr) particles. As of the literature, the σ-phase transition happens from the δ-ferrite, because it is a ferritic stabilizer which accumulates the chromium became rich Cr region. When there is no δ -ferrite present in the stainless steels, the σ -phase can potentially precipitate from γ –austenite [41].

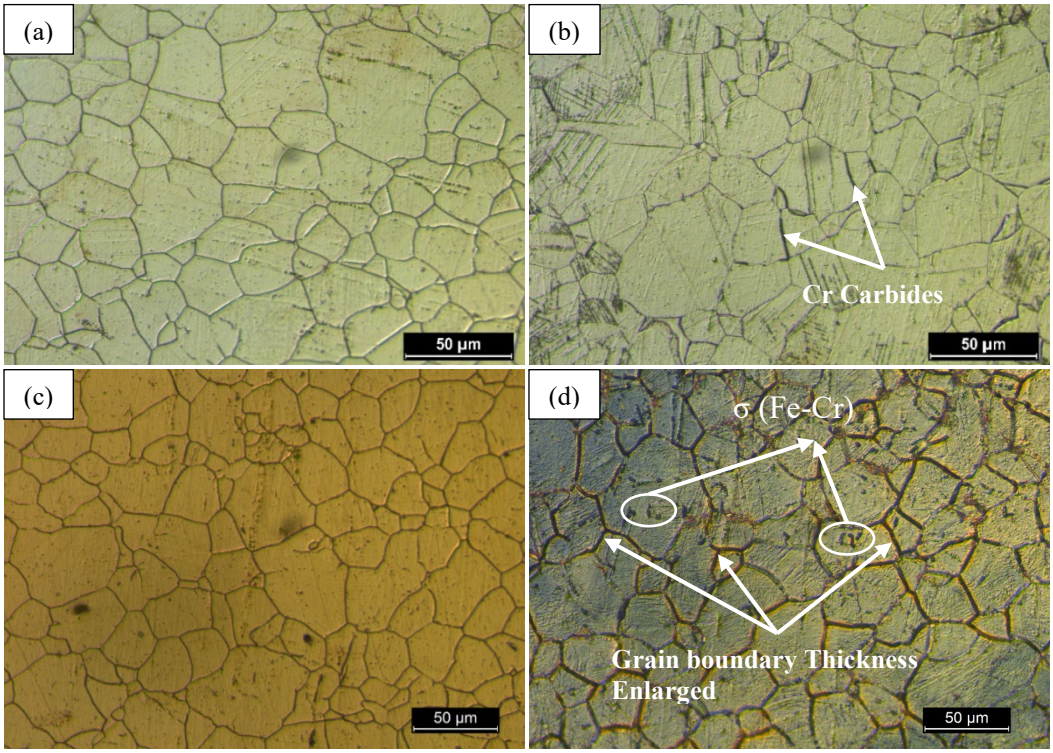

Figure 6: Photomicrographs of (a) AR, (b) SEN before the test, (c) AR1 and (d) SEN1 after the test (500x magnification)

Grain size is an important material characteristic, and it is denoted by ASTM 'G' number. For grain size, both samples can be determined by applying line intercept technique according to ASTM E112 [42]. Note that a large ASTM 'G' number indicates a smaller grain size and vice versa. Figure 7 summarizes the calculated ASTM 'G' number and average grain diameter (in µm) for four different sample conditions. Results shows that average grain diameter of SEN sample has slightly larger than AR sample, after the test also it was increased gradually. It can be assumed that the grain boundary migration happened if there is no delta-ferrite precipitation along the grain boundary. Under this circumstances, the previous grain boundary migrated quickly and formed new boundary as like double Y-shape, produced large grains [43]. Due to larger the grain size, the distance dislocation is longer that can take long time to move compared to shorter distance in case of small grains then the material loss its ductility. This can be assumed that, the austenite grain size is dependent on the volumetric density of nuclei induced by deformation [44]. Furthermore, while increasing the area of grain boundary it would be distribute more carbides along it and increases the sensitivity causes inter granular cracking corrosion when applied tensile stress [45], [46]. Due to overage of experimental work, occurred crack on SEN1 sample as shown in Figure 8 and it was a greater depth and intergranular. Finally, during the test the factors such as strain (0.05), temperature (90^{o}C) in long range and periodically used chloride (3.5wt.%) drips (rapid quenching) attributed to enhance the sensitization gradually leads to metal deformation occurred.

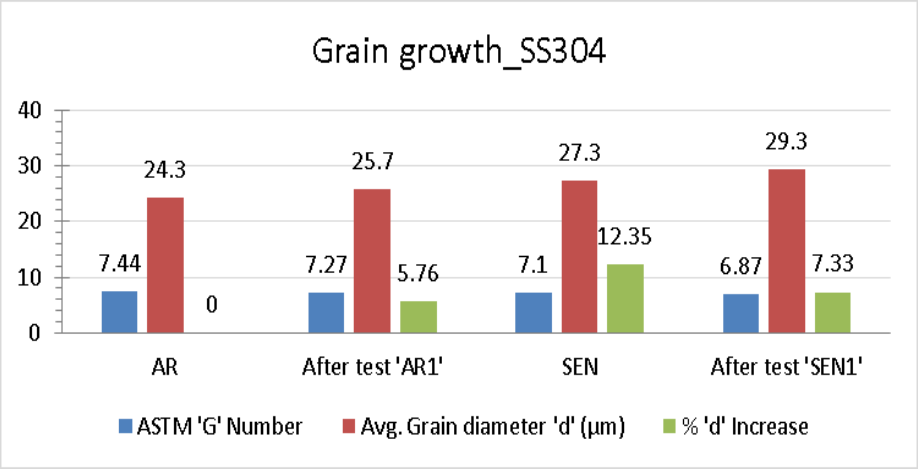

Figure 7: ASTM G number and average grain growth for as received and sensitized samples

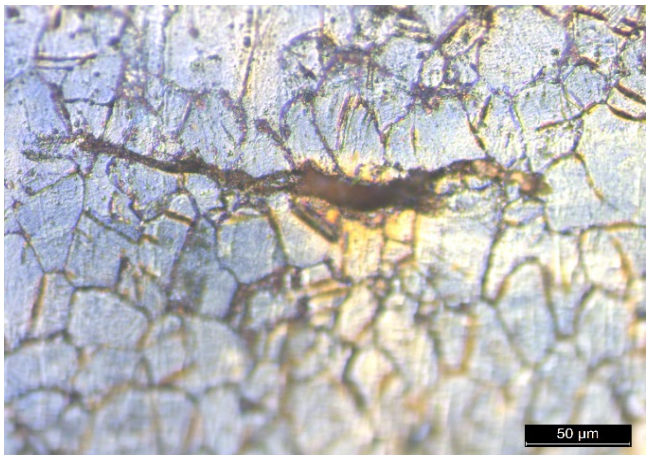

Figure 8: IGSCC on SS304 SEN1 sample under higher chloride concentration

FESEM observation:

For detailed investigation, the visuals taken by using FESEM for both SEN1 and AR1 shown in Figure 9. As the visuals characterized by seems to be an equiaxed grains with less carbide particles shown in Figure 9 (a), (d). Figure 9 (b), (e) representing brittle phase, there is almost dispersed the carbide particles along the grain boundary and it shown as a grooved grain structure due to the long range of experiment. Also observed the micro-fissures in the grain boundary as it might be developed by tensile stress and hence occurs the grain incoherence and it would supposed to intergranular cracking corrosion. In other side, Figure 9 (c) represents the flake carbide compounds along the grain boundary and the grain interior micro voids. Moreover, in case of tensile stress and temperature increased the flake carbides would disperse in the grain boundary. Moreover, as compared to SEN1 sample AR 1 structure has less plane defects (might be voids or stacking fault) with smooth grain surface.

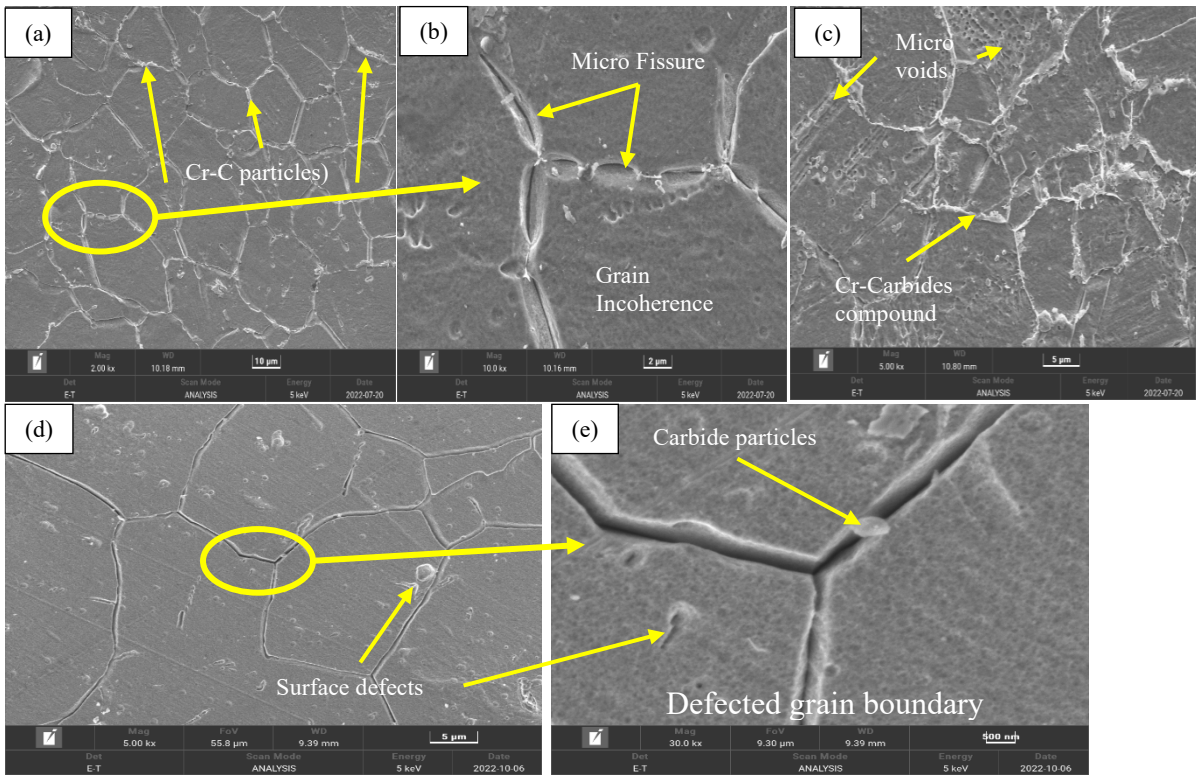

Figure 9: FESEM visuals and its characteristics of SEN1 (a), (b), (c) and AR1 (d), (e) tested samples

Finally observed the intergranular stress corrosion cracking (IGSCC), the crack seems to be more depth. It was distressed by the overage of experimental work and formed a lot of residual debris in the crack as shown in Figure 10. The metal dissolution in the crack interfaces causes by the applied parameters and those responsible for the development of metalloid debris along the crack. The initiation of crack takes place perpendicular to the applied tensile stress and the direction of dissemination slightly inclined. Here, the significant mechanism is the breakdown of interatomic bonding or decohesion along the grain boundary influenced by the mechanical load/tensile stress. At the crack tip, the strained interatomic bonds weaken by the absorbed chloride ions, hence the crack propagated and it depends on the loading condition, chloride concentration, exposure duration and temperature [47].

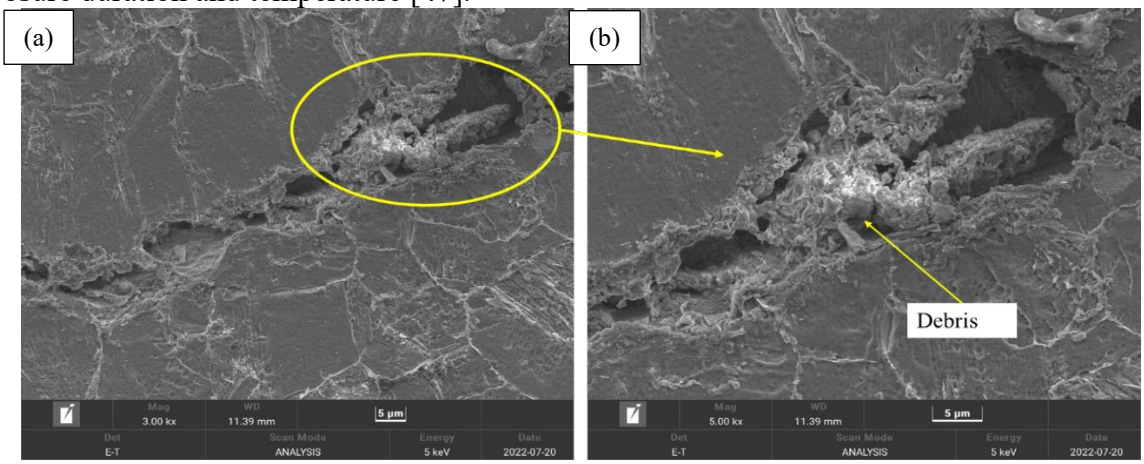

Figure 10: Overage tested sample (SEN1) FESEM images of (a) IGSCC at 3kx magnification and (b) IGSCC with debris at 5kx magnification

The energy dispersion spectrum (EDS) analysis was performed on the matrix surface (spectrum 22) and at grain boundary (spectrum 23) of SEN1 and AR1 as shown in Figure 11, contains the major elements of Fe, Cr, Ni and O. The phase of grain boundary in the SEN1 sample seems to be quite fragile. This phase exhibit frequently in austenitic stainless steels when used at temperatures more than 600 °C and owing to the corrosion products produced by stainless steels when Fe, Cr, and O are present [48]. From the spectrum 22, at the vicinity of grain boundary as rich in Cr and Fe than spectrum 23 and vice versa in AR1 sample. Assumed that where the chromium oxide is formed it might be initiate the pitting corrosion and leads to SCC when exposed to the residual or applied stress. Spectrum 23 at the grain boundary of SEN1, appears to be more sensitised and heavily oxidised than AR1. Sensitisation causes as result of chromium carbide precipitates at grain boundary. Chromium carbide precipitation creates chromium depleted zone in the vicinity of grain boundary. The precipitate happens continuously, the grain boundary becomes brittle and incoherence as leads to intergranular corrosion. Also, the cracks by residual stress propagates easily along the boundary [49]. In this case, observed sensitised samples are more possible to root the intergranular crack in the practice of drip test under the test parameters. The sensitised metal finally exposed as a result of crack propagation that are created at the oxide/metal interface.

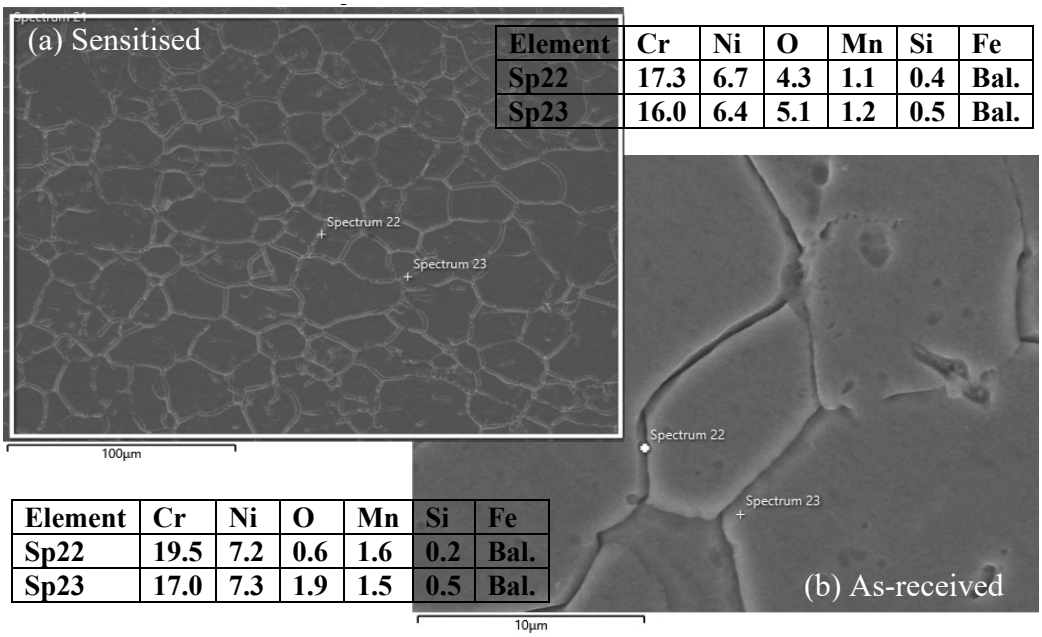

Element	Cr	Ni	O	Mn	Si	Fe
Sp22	17.3	6.7	4.3	1.1	0.4	Bal.
Sp23	16.0	6.4	5.1	1.2	0.5	Bal.

Element	Cr	Ni	O	Mn	Si	Fe
Sp22	19.5	7.2	0.6	1.6	0.2	Bal.
Sp23	17.0	7.3	1.9	1.5	0.5	Bal.

Figure 11: EDS spectrum analysis of element compositions of (a) SEN1 (b) AR1 tested samples

Conclusions

This work investigated the characteristics of CISCC on SS304 AR and SEN U-bend samples subjected to various chloride concentrations under perlite thermal insulation at 90ºC. The key findings can be summed up as follows:

- All the samples observed periodically and firstly detected the pitting corrosion on AR1 and SEN1 after 472 hours. SCC was detected on heat-sensitised sample under 3.5 wt% of NaCl solution after 1632 hours, while other sample were crack free.
- The sensitised sample had more CISCC susceptibility than as-received sample at higher chloride concentration. Grain size and micro-hardness has been increased in SEN1 than AR1 sample.

- Micro-fissures were detected in sensitised specimen's grain boundary by the dissolution of carbides in the action of tensile stress at 90ºC under higher NaCl concentration.
- In the extended test range, the sensitised sample experienced an intergranular crack with significant quantities of debris under 3.5 wt% of chloride concentration.

According to the practice of this work, physical inspection is a risk-based process and would be a difficult assignment. As result there will be a financial and production losses. For further enhancement, advise improving the design parameters and approach to non-destructive techniques (NDT) such as radiography, ultrasonic, eddy current testing, and acoustic emission technique.

Ethics Statement

The authors conducted and published this research in accordance with generally accepted standards of ethical behaviour.

Acknowledgement

The author would like to thank Ministry of Higher Education Malaysia (MOHE) for providing financial assistance under Fundamental Research Grant Scheme (FRGS/1/2/2020/TK0/UTP/03/2) and Universiti Teknologi PETRONAS for providing required facilities to conduct this research work.

References

[1] T. Michler, "Austenitic Stainless Steels," *Ref. Modul. Mater. Sci. Mater. Eng.*, no. June 2015, pp. 1–6, 2016, https://doi.org/10.1016/b978-0-12-803581-8.02509-1.

[2] S. M. Elsariti and Haftirman, "Behaviour of stress corrosion cracking of austenitic stainless steels in sodium chloride solutions," in *Procedia Engineering*, 2013, vol. 53, pp. 650–654, https://doi.org/10.1016/j.proeng.2013.02.084

[3] J. E. TRUMAN, "The influence of chloride content, pH and temperature of the test solution on the occurrence of stress corrosion cracking with austenitic stainless steel," *Corros. Sci. Pergamon Press. Print. Gt. Britain*, vol. 17, no. August 1976, pp. 737–746, 1977.

[4] NACE SP0198-2016, Control of Corrosion Under Thermal Insulation and Fireproofing Materials, vol. 2nd Ed., no. 21084. 2016.

[5] A. Bahadori, Thermal Insulation Handbook for the Oil, Gas, and Petrochemical Industries. 2014.

[6] F. De Vogelaere, "Corrosion Under Insulation," *Process Saf. Progress, Wiley InterScience-AIChE*, vol. 28, no. 1, pp. 30–35, 2009, https://doi.org/10.1002/prs.10276

[7] E. O. Eltai, F. Musharavati, and E. S. Mahdi, "Severity of corrosion under insulation (CUI) to structures and strategies to detect it," *Corros. Rev.*, no. 1988, pp. 1–12, 2019, https://doi.org/10.1515/corrrev-2018-0102

[8] B. R. Sanders, M. Production, J. R. Davis, and M. Park, *ASM Handbook- Volume 13C Corrosion : Environments and Industries*, vol. 13C. 2006.

[9] A. Almubarak, W. Abuhaimed, and A. Almazrouee, "Corrosion Behavior of the Stressed Sensitized Austenitic Stainless Steels of High Nitrogen Content in Seawater," *Int. J. Electrochem.*, vol. 2013, pp. 1–7, 2013, https://doi.org/10.1155/2013/970835

[10] M. Dahmen, K. D. Rajendran, and S. Lindner, "Sensitization of Laser-beam Welded Martensitic Stainless Steels," *Phys. Procedia*, vol. 78, no. August, pp. 240–246, 2015, https://doi.org/10.1016/j.phpro.2015.11.034.

[11] R. Parrott and H. Pitts, Chloride stress corrosion cracking in austenitic stainless steel. 2011.

[12] M. A. and E.-N. T. J. Bernard-Maxmillan Sim , Sai-Hong Tang, "Analyzing the Effects of Heat Treatment on SMAW Duplex Stainless Steel Weld Overlays," *Materials-MDPI*, pp. 1–12, 2022, https://doi.org/https://doi.org/10.3390/ma15051833

[13] İ. Demir, S. Başpınar, and E. Kahraman, "Production of insulations and construction materials from expanded perlite," *Springer Int. Publ.*, vol. 6, no. November, pp. 24–32, 2018, https://doi.org/10.1007/978-3-319-63709-9_3.

[14] J. W. Lee and K. E. Kee, "Experimental Study of Chloride-Induced Stress Corrosion Cracking (Ciscc) for Austenitic Sus 304L Under Thermal Insulation," *Platf. - A J. Eng.*, vol. 4, no. 2, pp. 31–43, 2020.

[15] Q. Cao *et al.*, "A Review of Corrosion under Insulation: A Critical Issue in the Oil and Gas Industry," *Metals (Basel).*, vol. 12, no. 4, pp. 1–24, 2022, https://doi.org/10.3390/met12040561

[16] U. K. Chatterjee, "Stress corrosion cracking and component failure: Causes and prevention," *Sadhana*, vol. 20, no. 1, pp. 165–184, 1995, https://doi.org/10.1007/BF02747288

[17] A. Bahadori, "Fundamentals of Corrosion in the Oil , Gas , and Chemical Industries," in *Corrosion and Materials Selection: A Guide for the Chemical and Petroleum Industries*, First Edit., John Wiley & Sons, Ltd, 2014, pp. 1–16.

[18] S. H. Khodamorad, N. Alinezhad, D. Haghshenas Fatmehsari, and K. Ghahtan, "Stress corrosion cracking in Type.316 plates of a heat exchanger," *Case Stud. Eng. Fail. Anal.*, vol. 5–6, pp. 59–66, 2016, https://doi.org/10.1016/j.csefa.2016.03.001

[19] U. NACE International, Houston, Texas, "International Measures of Prevention , Application , and Economics of Corrosion Technologies Study," 2016.

[20] A. C692-08, "Standard Test Method for Evaluating the Influence of Thermal Insulations on External Stress Corrosion Cracking Tendency of Austenitic Stainless," 1987.

[21] ASTM and E03-21, "Standard Guide for Preparation of Metallographic Specimens 1," 2001.

[22] A. International and A262-02a, "Standard Practices for Detecting Susceptibility to Intergranular Attack in Austenitic," 2002.

[23] ASTM and E572, "Standard Test Method for Analysis of Stainless and Alloy Steels by X-ray," *ASTM Int.*, vol. 03, no. June, pp. 1–10, 2003.

[24] ASTM Standard E8/E8M-13a, "'Standard Test Methods for Tension Testing of Metallic Materials,'" *ASTM Int.*, vol. i, pp. 1–27, 2013, [Online]. Available: http://www.astm.org/Standards/E8.htm.

[25] E384 and ASTM, "Microindentation Hardness of Materials 1," in *ASTM Standards*, vol. 14, 2002, pp. 1–24.

[26] ASTM A240, "ASTM A 240/A 240M – 04. Standard Specification for Chromium and Chromium-Nickel Stainless Steel Plate, Sheet, and Strip for Pressure Vessels and for General Applications," *ASTM Int.*, vol. i, p. 12, 2004, [Online]. Available: http://www.ussa.su/gosts2/ASTM_A240.PDF

[27] A. International and G30-97, "Standard Practice for Making and Using U-Bend Stress-Corrosion Test," in *ASTM Standards*, vol. i, no. Reapproved, 2009, pp. 1–7.

[28] A. . Dana, "Stress- Corrosion Cracking of Insulated Austenitic Stainless Steel," *ASTM Bull.*, pp. 46–52, 1957.

[29] C610 and ASTM, "Standard Specification for Molded Expanded Perlite Block and Pipe Thermal," in *ASTM Standards*, vol. 04, 2000, pp. 1–4.

[30] C585 and ASTM, "Standard Practice for Inner and Outer Diameters of Rigid Thermal Insulation for Nominal Sizes of Pipe and Tubing (NPS System) 1," in *ASTM Standards*, vol. 90, no. Reapproved, 2004, pp. 1–9.

[31] AAAMSA, THERMAL INSULATION Incorporating the Architectural Glass Industry Incorporating the Architectural Glass Industry, no. April. 2001.

[32] D1193 and ASTM, "Reagent Water 1," *ASTM Int.*, vol. 51, no. 7916, pp. 1–3, 2001.

[33] G44 and ASTM, "Standard Practice for Exposure of Metals and Alloys by Alternate Immersion in," *ASTM Int.*, vol. 11, no. Jan, pp. 1–4, 2000.

[34] P. Street, "Metastable pitting corrosion of stainless steel and the transition to stability," *Philos. Trans. R. Soc. London. Ser. A Phys. Eng. Sci.*, vol. 341, no. 1662, pp. 531–559, 1992, https://doi.org/10.1098/rsta.1992.0114.

[35] S. Caines, F. Khan, J. Shirokoff, and W. Qiu, "Journal of Loss Prevention in the Process Industries Experimental design to study corrosion under insulation in harsh marine environments," *J. Loss Prev. Process Ind.*, vol. 33, pp. 39–51, 2015, https://doi.org/10.1016/j.jlp.2014.10.014

[36] P. Wang, Y. Zhang, and D. Yu, "Microstructure and mechanical properties of pressure-quenched SS304 stainless steel," *Materials (Basel).*, vol. 12, no. 2, pp. 1–9, 2019, https://doi.org/10.3390/ma12020290

[37] P. R. Rios and A. F. Padilha, "Precipitation From Austenite," *Ref. Modul. Mater. Sci. Mater. Eng.*, no. February 2015, pp. 1–8, 2019, https://doi.org/10.1016/b978-0-12-803581-8.02522-4.

[38] G. Yin, Y. Li, J. Sun, and J. Chen, "Effect of Heat Treatment Temperature on Mechanical Properties of the AISI 304 Stainless Steel," *Int. J. Innov. Res. Sci. Eng. Technol.*, vol. 3, no. 2, pp. 9516–9520, 2014, https://doi.org/10.7521/j.issn.0454-5648.2014.03.17

[39] R. W. Armstrong, "60 years of hall-petch: Past to present nano-scale connections," *Mater. Trans.*, vol. 55, no. 1, pp. 2–12, 2014, https://doi.org/10.2320/matertrans.MA201302.

[40] M. M. Louwerse and A. C. Graesser, "Macrostructure," in *Metallography: Principles and Practice (#06785G)*, 2006, pp. 426–429.

[41] C.-C. Hsieh and W. Wu, "Overview of Intermetallic Sigma (σ) Phase Precipitation in Stainless Steels," *ISRN Metall.*, vol. 2012, no. 4, pp. 1–16, 2012, https://doi.org/10.5402/2012/732471

[42] ASTM E112, "Standard Test Methods for Determining Average Grain Size," 2010.

[43] Y. Komizo, "Correlation of delta-ferrite precipitation with austenite grain growth during annealing of steels," *Philos. Mag. Lett.*, vol. 91, no. July, pp. 491–497, 2011, https://doi.org/10.1080/09500839.2011.587464

[44] P. Kral *et al.*, "Creep Resistance of S304H Austenitic Steel Processed by High-Pressure Sliding," *Materials (Basel).*, vol. 15, no. 1, 2022, https://doi.org/10.3390/ma15010331.

[45] M. A. Mohtadi-Bonab, "Effects of different parameters on initiation and propagation of stress corrosion cracks in pipeline steels: A review," *Metals (Basel).*, vol. 9, no. 5, pp. 1–18, 2019, https://doi.org/10.3390/met9050590

[46] S. K. Pradhan, T. S. Prithiv, and S. Mandal, "Through-thickness microstructural evolution during grain boundary engineering type thermomechanical processing and its implication on sensitization behavior in austenitic stainless steel," *Mater. Charact.*, vol. 134, no. July, pp. 134–142, 2017, https://doi.org/10.1016/j.matchar.2017.10.014

[47] Woodhead Publishing Limited, *Stress corrosion cracking: Theory and practice*. Woodhead Publishing Limited, 2011.

[48] P. P. Psyllaki, G. Pantazopoulos, and A. Pistoli, "Degradation of stainless steel grids in chemically aggressive environment," *Eng. Fail. Anal.*, vol. 35, pp. 418–426, 2013, https://doi.org/10.1016/j.engfailanal.2013.04.016

[49] M. W. A. Rashid, M. Gakim, Z. M. Rosli, and M. A. Azam, "Formation of Cr23C6 during the sensitization of AISI 304 stainless steel and its effect to pitting corrosion," *Int. J. Electrochem. Sci.*, vol. 7, no. 10, pp. 9465–9477, 2012.